Available online at www.sciencedirect.com
ScienceDirect
Journal of the European Ceramic Society 27 (2007) 3867–3872
www.elsevier.com/locate/jeurceramsoc

Varistors based in the $ZnO–Bi_2O_3$ system: Microstructure control and properties

Marco Peiteado *, José F. Fernández, Amador C. Caballero

Department of Electroceramics, Instituto de Cerámica y Vidrio, CSIC, 28049 Madrid, Spain

Available online 23 March 2007

Abstract

The present contribution deals with the development of an empirical approach that will describe the evolution of the breakdown voltage in ZnO-based varistors as a function of the sintering variables. This relationship is described through the kinetic analysis of the grain growth process. It is found that for a certain range of sintering conditions the varistor breakdown voltage could be calculated from the average size that zinc oxide grains achieve, provided that the varistor microstructure evolves in a gradual and controlled manner and the distribution of the electrical interphases remains stable.

Keywords: ZnO; Varistors; Grain growth; Sintering kinetics; Electrical properties

1. Introduction

ZnO based varistors exhibit highly nonlinear current–voltage characteristics which find application in the field of protection against transient voltage surges.[1–3] In doped ZnO ceramics *non-linearity coefficients* as high as $\alpha \sim 70$ can be achieved with α being defined as a local approximation $I \sim V^{\alpha}$ to the electrical current–voltage response.[2] In standby, the varistor is subjected to a voltage below its characteristic *breakdown voltage* and only a *leakage current* pass through the bulk specimen; during a transient surge the voltage between electrodes exceeds the breakdown voltage and the varistor becomes highly conductive diverting the current to ground and so protecting the circuit. The non-linear response originates on its polycrystalline microstructure and more specifically on detailed processes occurring at the grain/grain interfaces. By proper doping, the near grain boundary region becomes highly resistive while the grain interior turn into conductive, and electrostatic potential barriers build up at the grain boundaries due to charges being trapped at interface states.[4–6] In this way, varistors are equivalent to back-to-back Zener diodes but with much greater current and energy handling capabilities that make them suitable for high voltage applications.

Typical formulation of ZnO based varistors comprises zinc oxide with small amounts of other metal oxides, such as Bi_2O_3, Sb_2O_3, Cr_2O_3, MnO_2 and CoO among others.[7] Sintering of the green compacts takes place in the presence of a liquid phase and the microstructure thus formed consists of ZnO semiconductor grains with a bismuth-rich second phase at triple and multiple junctions that percolates through the whole ceramic body. Monoatomic layers of bismuth excess and oxygen segregated at the grain boundaries are responsible for the electrical activity of the interfaces.[8] Besides particles of a secondary $Zn_7Sb_2O_{12}$ spinel-type phase are also located at grain boundaries and multiple junctions. The formation of this spinel phase and the release of the liquid take place on sintering through reactions between ZnO and the Bi_2O_3 and Sb_2O_3 dopants.[9] More specifically in a recent work we have found that the thermal evolution of this ternary system involves two simultaneous reaction paths, originated both on the partial oxidation of Sb_2O_3 to Sb_2O_4.[10] In one of these paths, part of the oxidized antimony reacts with zinc and bismuth oxides to form an intermediate $Zn_2Bi_3Sb_3O_{14}$ pyrochlore-type phase; around 900 °C this pyrochlore decomposes to form liquid Bi_2O_3 and a spinel phase. In the other path, the remaining antimony reacts with ZnO leading to a tri-rutile $ZnSb_2O_6$ phase which above 800 °C forms more spinel-type phase. As a result a functional microstructure is obtained in which the liquid phase is promoting the densification of the ceramic and the growth of ZnO grains; the spinel particles on the other hand, by acting as inclusions that pin the grain boundary motion, control the ZnO grain growth.

* Corresponding author at: Advanced Materials Department, Jozef Stefan Institute, Jamova 39, 1000 Ljubljana, Slovenia. Tel.: +386 1 4773629; fax: +386 1 4773875.
E-mail address: marco.peiteado@ijs.si (M. Peiteado).

0955-2219/$ – see front matter © 2007 Elsevier Ltd. All rights reserved.
doi:10.1016/j.jeurceramsoc.2007.02.046

From the above it is deduced that the two essential features of varistor microstructure determining its non-linear response are the formation of Bi-enriched active grain boundaries as well as a controlled ZnO grain size. Particularly, the breakdown voltage of the varistor could be related to the size of zinc oxide grains; provided that the microstructure of the ceramic remain homogenous with regard to the nature and distribution of phases, the breakdown voltage decreases linearly as the average size of ZnO grains increases[11]:

$$V_B = \frac{m \cdot d}{G \cdot V_{gb}} \quad (1)$$

where V_B is the breakdown voltage, d the sample thickness or distance between electrodes, G the average size of ZnO grains, V_{gb} the voltage across a single potential barrier or a single grain boundary, and the coefficient m is actually averaging the potential barrier distribution. This last parameter comes from the fact that in real systems there is considerable evidence for substantial variations in the performance of individual varistor grain boundaries as well as inactive grain boundaries that do not show varistor effect at all.[12] According to this expression, ZnO grains become the *construction blocks* from which different devices could be produced; to meet the requirement for a given technological application, changes in the nominal breakdown voltage could be achieved either by increasing the varistor thickness or, for a given thickness, by changing the average size of ZnO grains. However, the first alternative is usually impeded by the specimen geometry, so in most applications the breakdown voltage has to be fitted by strictly controlling the size of ZnO grains. Furthermore, since the final size of ZnO grains is defined by the applied sintering temperature and time, one could expect that the breakdown voltage could be fitted by controlling these variables. This gives a special significance to the grain growth kinetics and activation analyses: for a given composition the connection between the couple temperature-time and the size of zinc oxide grains is defined by the grain growth activation analysis. At the final stage of sintering, densification has proceed to a large extent and the predominant mechanism is the coarsening of microstructure by grain growth.[13] In dense polycrystalline solids this grain growth process could be split into two major contributions; the first one corresponding to the growth experimented during heating at a constant heating rate and the second one taking place under isothermal conditions during the soaking time:

$$G(T,t) = A\ \exp\left\{\frac{-Q}{RT}\right\} + B \cdot t^{1/n} \quad (2)$$

where $G(T,t)$ will be the expected grain size for a sintering temperature T and a soaking time t, n and Q are, respectively, the kinetic exponent and the activation energy of the grain growth process, and A and B are constants that should be evaluated from fitting the experimental data of the kinetic and the activation analyses.

If we now combine Eqs. (1) and (2), an empirical expression is obtained which directly relates the varistor breakdown voltage with the sintering temperature and time variables:

$$V_B = m\frac{d \cdot V_{gb}}{A \cdot t^{1/n} + B\exp^{-Q/RT}} \quad (3)$$

As can be seen this approach involves up to five variables. These variables can be worked out from a few numbers of experiments in which different sintering temperature-time couples are combined, but, once solved, it is expected that the prediction of the breakdown voltage can be extended to a wider range of sintering temperatures and times.

2. Experimental

As mentioned, for the breakdown voltage to be quantitatively predicted as a function of the sintering conditions, there is one restrictive condition: the microstructure of the ceramic should remain homogenous with regard to the nature and distribution of phases. From an experimental point of view this is straightly related to the processing strategy employed to obtain the ceramic powder. Pursuing this objective, up to five different processing strategies based on both solid oxide powders and chemical routes were analyzed. In all cases a standard varistor composition was used comprising ZnO (95.5 mol%), Bi_2O_3 (0.5%), Sb_2O_3 (1.5%), SnO_2 (0.5%), Co_3O_4 (0.5%), MnO (0.5%) and NiO (1.0%) in mol%. For the batch labeled VP1, the varistor powder was obtained following a classical mixed oxide route including ball milling for 2 h in ethanol; in this system the sintering reactions take place as described above. The second batch, VP2, was prepared in the same way but with the Sb_2O_3 being substituted for the equivalent amount of the previously synthesized $Zn_7Sb_2O_{12}$ spinel phase; as a result no reactions will occur during the heating of this powder, and the liquid phase will appear at lower temperatures, around 740 °C, from the eutectic reaction between ZnO and un-reacted Bi_2O_3.[14] In batch number three, VP3, the oxides are mixed and then subjected to a previous calcination step at 950 °C/1 h; in this powder the particles are pre-reacted and the sintering reactions have progressed to a certain extent. Finally to improve the reactivity of the particles, two chemical routes were also tested. One of them, VP4, involves the co-precipitation of bismuth and antimony cations onto a ZnO aqueous suspension. In the other one, VP5, the powder was prepared by co-precipitating all the components of the formulation via a citrate-route (Pechini method).[15] Table 1 resumes the main characteristics of each analyzed strategy.

Table 1
Main characteristics of the different processing strategies analyzed in this work

Material	Strategy	Objective
VP1	Mixed oxides	Reactions during sintering
VP2	Mixed oxides and spinel instead of Sb_2O_3	No reactions. Formation of liquid at 740 °C (eutectic ZnO–Bi_2O_3)
VP3	Mixed oxides and calcination step at 950 °C/1 h	Pre-reacted system
VP4	Co-precipitation of Bi and Sb precursors onto ZnO aqueous suspension	High reactive system
VP5	Pechini method	High reactive system

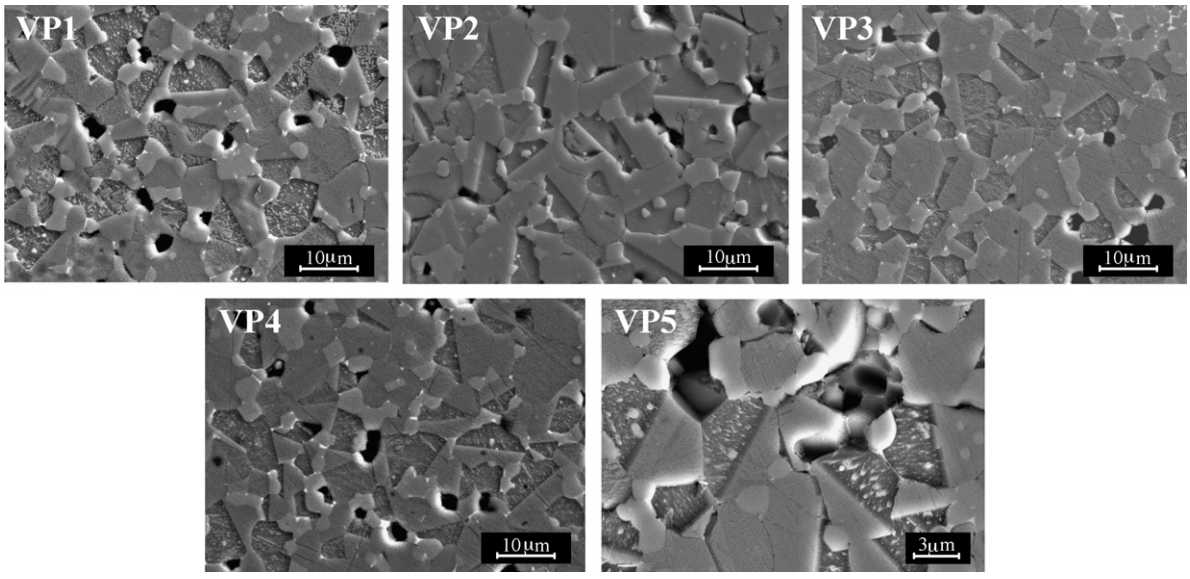

Fig. 1. FE-SEM micrographs of samples of the five varistor batches sintered at 1180 °C for 2 h.

Green compacts of the five varistor powders were uniaxially pressed at 80 MPa into pellets of approximately 12 mm in diameter and thickness and then subjected to identical sintering cycles. Firing of the pressed bodies was carried out in air for sintering temperatures ranging from 1140 to 1240 °C and soaking times from 0 to 8 h. Densities of sintered samples were measured using the water-immersion method of Archimedes and in all cases values of >97% of the theoretical density were achieved. For microstructural observations the surfaces of the samples were polished and chemically etched with oxidizing HCl, and field emission scanning electron microscopy (FE-SEM) was carried out using Hitachi S-4700 microscope. ZnO grain size was determined from FE-SEM micrographs by an image processing and analysis program. More than 800 grains were taken into account. For electrical characterization, sintered samples were cut into 3 mm thick discs and Ag electroded. Standard I–V measurements were carried out using a dc power multimeter Keithley 2410. The varistor breakdown voltage V_B was estimated at a current density of 5 mA/cm^2. The density of leakage currents J_L was measured at a voltage corresponding to the 85% of the breakdown voltage. Finally the non-linear coefficient a was measured in the current density range between 5 and 20 mA/cm^2.

3. Results and discussion

Fig. 1 depicts the SEM micrographs of samples of each batch after sintering at 1180 °C for 2 h. At this temperature, a similar microstructure is obtained in all cases with the only appreciable differences coming from the average size of ZnO grains. This is more clearly illustrated in data of Table 2 which resumes the ZnO grain size. As observed the smallest size corresponds to the sample prepared by the Pechini method (VP5), which is in agreement with the high reactivity of the particles obtained by this route. Besides Table 2 also shows that batches VP3 and VP4 lead to a more controlled grain size than that of the other two powders prepared by mixing the oxides.

But, with regards to the homogeneity of the systems, the strongest differences appear when measuring the electrical behavior of the samples. As can be seen in Fig. 2, when sintering at 1180 °C for 2 h the first four batches show a similar shape of the I–V curve, with a sharp transition from the zone of low currents to the non-linear region. Only sample of batch VP5 shows a much rounded transition, which is an indication of a poor electrical response. This is confirmed when measuring the varistor functional parameters. Table 3 shows indeed a low non-linear coefficient α as well as a very high level of leakage currents in sample VP5 sintered at 1180 °C/2 h. Such a poor behavior in this system should be attributed to the small grain size and high reactivity of its particles, making this powder to

Table 2
Average ZnO grain size of samples sintered at 1180 °C/2 h

Material	G_{ZnO} (±0.5 μm)
VP1	7.0
VP2	7.7
VP3	6.3
VP4	6.1
VP5	4.7

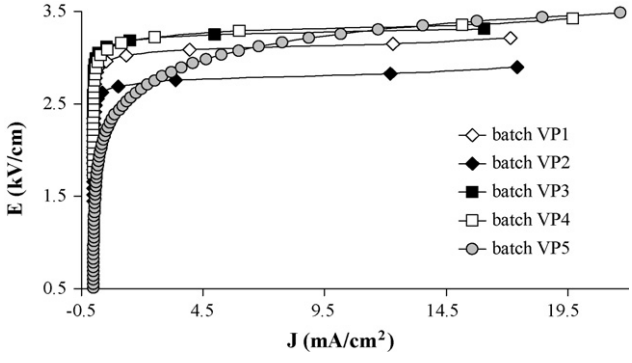

Fig. 2. I–V curves of samples sintered at 1180 °C/2 h.

Table 3
Electrical properties of samples sintered at 1180 °C/2 h (batch VP5 was also sintered at 950 °C/4 h (marked with asterisk))

Material	V_B (V)	α	J_L (mA/cm^2)
VP1	3096	54	0.026
VP2	2777	48	0.033
VP3	3245	55	0.011
VP4	3274	46	0.049
VP5	2981	10	1.406
VP5*	16108	34	0.303

The measurement uncertainties were of 3% for the breakdown voltage V_B, of 5% for α and of 25% for the density of leakage currents J_L.

Table 4
Evolution of ZnO average grain size (G_{ZnO}) and breakdown voltage (V_B) of samples of batch VP3 with the sintering variables

Sintering conditions		G_{ZnO} (±0.5 μm)	V_B (V)
t = 2 h	1140 °C	5.3	3176
	1160 °C	5.8	2952
	1180 °C	6.3	2777
	1200 °C	6.9	2590
	1220 °C	7.4	2460
T^a = 1180 °C	0 h	5.1	3452
	4 h	7.0	2377
	8 h	8.4	2166

sinter at lower temperatures. Being this so, any excess of temperature would only lead to a deterioration of the microstructure and consequently of the electrical properties. Thus when sintering this batch at 950 °C for 4 h, its electrical response, although still far from that of the other systems, improves noticeable with an α value above 30 (Table 3). Besides its breakdown voltage is remarkably high, up to 16 kV. This is due to a really smaller grain size, now close to only 1.4 μm at this 950 °C/4 h. However, from the point of view of the energy handling capability, this will represent a serious problem in bulk samples, particularly in the case of high voltage applications where a high level of energy is involved. Hence although this processing strategy could find utility in low voltage circuits, we can discard it now for our present objective.

Table 3 also shows that the problems arising with the Pechini method can be overcome with the other chemical route, the co-precipitated one (VP4). However it is also observed that the electrical response attained with this strategy does not improve substantially the behavior obtained with the solid oxide powders. Hence since the nature of the co-precipitation technique involves a more sophisticated processing, we finally focused our interest on the three systems prepared by mixing the oxides. In a previous contribution we found that the smoothest variation of ZnO grain size with the sintering conditions was obtained for that one including the previous calcination step (VP3).[16] This obeys to a higher degree of homogeneity in this batch. Therefore in our search for a strategy leading to an improved grain growth control, the solid oxide processing with the incorporation of a pre-reaction step shows the most interesting results. According to this, the activation analyses were then carried out on samples of this batch VP3.

3.1. Activation analysis

Table 4 first shows the evolution of ZnO grain size and the breakdown voltage as a function of the sintering conditions for samples of batch VP3. As expected the average size of zinc oxide grains increases as the sintering temperature and soaking time are increased. Parallel the breakdown voltage decreases. With these data and following the kinetic studies of Senda and Bradt,[17] a kinetic exponent of $n = 6.4$ was obtained. There has not been a satisfactory explanation for any mechanism of grain boundary migration with a grain growth exponent higher than 5, even though a similar behavior has been previously observed.[18,19] In fact, the physical significance of the n values determined from grain growth data can be certainly doubtful, primary because the many approximations used in the derivation of the kinetic equations. Furthermore the fitting of experimental data to produce n values that are integer numbers may not be realistic because the occurrence of simultaneous mechanisms is expected to give n values that are not integers. Even so, to complete the activation analysis the kinetic exponent should be fitted to an integer number. In doing so, Senda and Bradt first fitted an n value of 6 from different slopes as the more reasonably for ZnO ceramics doped with antimony oxide.[18] Besides, in the unique available paper to date concerning on grain growth kinetics for a ZnO–Bi_2O_3–Sb_2O_3-based varistor composition, an average value of 6 for the kinetic exponent is also reported.[20] This value also seems to be in good agreement with our experimental results so finally we took $n = 6$ for our varistor system.

With the value of the kinetic exponent, the activation energy Q for the grain growth process can be determined from the slopes of the Arrhenius plots $\log(G^n/t)$ versus $1/T$.[17] A value of $Q = 613 \pm 20$ kJ/mol was obtained. It is consistently larger than that of pure ZnO (224 ± 16 kJ/mol),[17] which evidences an inhibition of grain growth in this varistor system. Following, with the values of n and Q, the constants A and B were calculated from the fitting of the experimental data in Eq. (1) leading, respectively, to $A = 1.54$ μm s$^{-1/6}$ and $B = 1.25 \times 10^{22}$ μm. In the same way the value of the correction factor m was obtained by introducing the experimental data of G and V_B (Table 4) on Eq. (2); assuming a constant value of $V_{gb} = 3.2$ V for the voltage across a single grain boundary,[12] a value of $m = 0.68$ was obtained for the samples of this batch VP3.

Once all the variables of the proposed approach are obtained, the range of application must be evaluated. Table 5 compares the breakdown voltage calculated from Eq. (3) with that measured experimentally. More specifically, data in bold represent those theoretical values that reproduce the experimental ones with a deviation margin below 10%. The study has been extended to a wider range of sintering conditions than the strictly used in obtaining the variables of the approach and as can be seen the prediction widely fits to these samples of batch VP3. Only in the farthest experiments, that is low sintering temperatures with short soaking times as well as high temperatures with long dwells, the prediction is not working so suitably. All these experiments have been repeated for several times to find out that at

Table 5
Range of application of the empirical approach developed to determine the varistor breakdown voltage as a function of the sintering conditions (values in volts)

VP3 (°C)	0 h		2 h		4 h		8 h	
	$V_{exp.}$	$V_{calc.}$	$V_{exp.}$	$V_{calc.}$	$V_{exp.}$	$V_{calc.}$	$V_{exp.}$	$V_{calc.}$
1140	5526	4898	3802	**3761**	3492	**3343**	3149	**3008**
1160	4492	**4680**	3481	**3570**	3254	**3240**	2911	**2885**
1180	4262	**4298**	3245	**3343**	3035	**3052**	2734	**2735**
1200	3989	**3829**	3155	**3052**	2863	**2771**	2471	**2538**
1220	3417	**3191**	2860	**2666**	2684	**2452**	2028	2265

Data in bold correspond to those calculated values of the breakdown voltage ($V_{calc.}$) that reproduce the experimental ones ($V_{exp.}$) with a deviation margin below 10%.

low sintering temperatures with short soaking times there is a lack of reproducibility which can be detected even inside one single sample. This is clearly depicted in the I–V curves of Fig. 3 which compares the electrical response of different slices of one sample sintered at 1140 °C for 0 h and one sintered at 1180 °C for 2 h. While the discs of the sample sintered at 1180 °C give place to practically the same behavior, those of the sample sintered at 1140 °C lead to a high scattering of the electrical data. The microstructural analysis of these samples showed that this lack of reproducibility arising at low sintering temperatures with short soaking times comes from macroscopic heterogeneities in the sintered samples; these low-energy treatments cannot avoid the development of large accumulations of secondary phases as that observed in Fig. 4, that gather on cooling and lead to the formation of preferential conduction paths inside the material. This finally results in the dispersion of the measurement depending on the number and size of these *clusters* of secondary phases in the varistor specimen. An increase in the energy supplied to the system however reduces the presence of these accumulations and consequently increases the macroscopic homogeneity.

On the other hand the degradation on the electrical response at high temperatures with extended dwell times evidence either a decrease in the height of the potential barriers or a decrease in the number of active boundaries. Such behavior is believed to be originated on a bismuth loss by vaporization, since as previously mentioned one of the essential features determining the varistor non-linear behavior is the formation of Bi-enriched active grain boundaries. In a previous contribution we observed a bismuth loss up to 60% when sintering these materials at 1240 °C for 4 h,[21] with the subsequent deterioration of the electrical response.

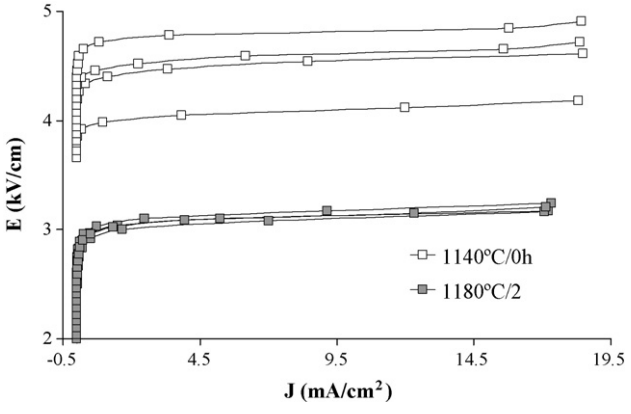

Fig. 3. I–V response of different slices of samples of batch VP3 sintered at 1140 °C/0 h and 1180 °C/2 h.

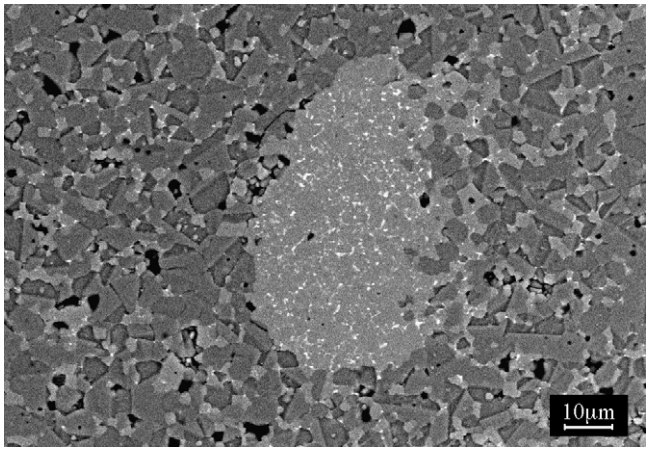

Fig. 4. SEM micrograph of sample of batch VP3 sintered at 1140 °C for 0 h, showing a large accumulation of secondary phases; dark-grey zones correspond to ZnO grains, whereas light-grey regions correspond to the spinel-type grains and white brilliant regions to the Bi-rich phases.

4. Conclusions

Different processing strategies based on both solid oxide powders and chemical routes have been analysed in the search of a highly homogeneous system that will allow a better control of the varistor electrical properties. Solid oxide processing with the incorporation of a pre-reaction step shows the most interesting results for bulk samples. Then it is possible to obtain an empirical expression that quantitatively predicts the varistor breakdown voltage as a function of the sintering conditions. The parameters defining this expression can be obtained from a few numbers of experiments, and the final range of temperatures and times over which this expression can be successfully applied is again a function of the microstructure homogeneity.

Acknowledgements

This work has been conducted within the CICYT MAT 2004-04843-C02-01 project. The authors would like to express their gratitude to the company INAEL S.A. (Toledo, Spain) for the fruitful cooperation.

References

1. Matsuoka, M., Nonohmic properties of zinc oxide ceramics. *Jpn. J. Appl. Phys.*, 1971, **10**(6), 736–746.
2. Clarke, D. R., Varistor ceramics. *J. Am. Ceram. Soc.*, 1999, **82**(3), 485–502.
3. Gupta, T. K., Application of zinc oxide varistors. *J. Am. Ceram. Soc.*, 1990, **73**(7), 1817–1840.
4. Castro, M. S., Nunez, G. M., Resasco, D. E. and Aldao, C. M., Prebreakdown conduction in ZnO varistors. *J. Am. Ceram. Soc.*, 1992, **75**(4), 800–804.

5. Fernández-Hevia, D., Peiteado, M., De Frutos, J., Caballero, A. C. and Fernández, J. F., Wide range dielectric spectroscopy of ZnO-based varistors as a function of sintering time. *J. Eur. Ceram. Soc.*, 2004, **24**(6), 1205–1208.
6. Leach, C., Grain boundary structures in zinc oxide varistors. *Acta Mater.*, 2005, **53**(2), 237–245.
7. Peiteado, M., Zinc oxide-based ceramic varistors. *Bol. Soc. Esp. Ceram. V*, 2005, **44**(2), 77–87.
8. Greuter, F., Electrically active interfaces in ZnO varistors. *Solid State Ionics*, 1995, **75**, 67–78.
9. Leite, E. R., Nobre, M. A. L., Longo, E. and Varela, J. A., Microstructural development of ZnO varistors during reactive liquid phase sintering. *J. Mater. Sci.*, 1996, **31**(20), 5391–5398.
10. Peiteado, M., De la Rubia, M. A., Fernández, J. F. and Caballero, A. C., Thermal evolution of ZnO–Bi_2O_3–Sb_2O_3 system in the region of interest for varistors. *J. Mater. Sci.*, 2006, **41**(8), 2319–2325.
11. Hozer, L., Metal-oxide varistors. *Semiconductor Ceramics: Grain Boundary Effects*. Polish Scientific Publishers, Warszawa, Poland, 1994, p. 44–109.
12. Olsson, E. and Dunlop, G. L., Characterization of individual interfacial barriers in a ZnO varistor material. *J. Appl. Phys.*, 1989, **66**(8), 3666–3675.
13. Kang, S. J. L. and Jung, Y. I., Sintering kinetics at final stage sintering: model calculation and map construction. *Acta Mater.*, 2004, **52**(15), 4573–4578.
14. Serena, S., De la Rubia, M. A., Caballero, A. C. and Caballero, Y. C., Thermodynamic study of the rich-Bi_2O_3 region of the Bi_2O_3–ZnO system. *Bol. Soc. Esp. Ceram. V*, 2006, **45**(3), 150–153.
15. Lorentz, A., Ott, J., Harrer, M., Preissner, E. A., Whitehead, A. H. and Schreiber, M., Modified citrate gel techniques to produce ZnO-based varistors (Part I. Microstructural characterization). *J. Electroceram.*, 2001, **6**(1), 43–54.
16. Peiteado, M., Fernández, J. F. and Caballero, A. C., Processing strategies to control grain growth in ZnO based varistors. *J. Eur. Ceram. Soc.*, 2004, **25**(12), 2999–3003.
17. Senda, T. and Bradt, R. C., Grain growth in sintered ZnO and ZnO–Bi_2O_3 ceramics. *J. Am. Ceram. Soc.*, 1990, **73**(1), 106–114.
18. Senda, T. and Bradt, R. C., Grain growth of zinc oxide during the sintering of zinc oxide-antimony oxide ceramics. *J. Am. Ceram. Soc.*, 1991, **74**(6), 1296–1302.
19. Dey, D. and Bradt, R. C., Grain growth of ZnO during Bi_2O_3 liquid-phase sintering. *J. Am. Ceram. Soc.*, 1992, **75**(9), 2529–2534.
20. Chen, Y. C., Shen, Y. C. and Wu, L., Grain growth processes in ZnO varistors with various valence states of manganese and cobalt. *J. Appl. Phys.*, 1991, **62**(12), 8363–8367.
21. Peiteado, M., De la Rubia, M. A., Velasco, M. J., Valle, F. J. and Caballero, A. C., Bi_2O_3 vaporization from ZnO-based varistors. *J. Eur. Ceram. Soc.*, 2005, **25**(9), 1675–1680.